ELSEVIER

International Journal of Heat and Fluid Flow 22 (2001) 279–286

International Journal of HEAT AND FLUID FLOW

www.elsevier.com/locate/ijhff

Fluid flow and heat transfer around a rectangular cylinder with small inclined angle (the case of a width/height ratio of a section of 5)

T. Igarashi *, Y. Mayumi

Department of Mechanical Engineering, National Defense Academy, 1-10-20 Hashirimizu, Yoskosuka 239-0811, Japan

Abstract

Experimental studies on fluid flow and heat transfer characteristics around a rectangular cylinder at the same angle of attack were carried out for Reynolds number in the range 2500–12 800. In the experiment, width/height ratio of the cylinder was chosen as 5.0 and the angle of attack was varied over the range 0–20°. For $\alpha = 0°$, the cylinder axis was aligned with the flow, the separated shear layers reattached to the top and bottom surfaces intermittently. For $\alpha \geqq 5°$, the lower shear layer reattached to the lower surface. The reattached flow becomes turbulent for $\alpha < 15°$, while the flow remains laminar for $\alpha > 15°$. A clear understanding of the local heat transfer coefficients around the cylinder can be obtained in relation with the flow characteristics. The local heat transfer coefficients on the reattachment surface and on the upper and lee surfaces can be represented by the same empirical relation, $Nu = CRe^{2/3}$. The constant C decreases with increases in α for $\alpha > 5°$. Finally, maximum average heat transfer is achieved for α values between 0° and 5°.

Keywords: Forced convection; Heat transfer; Rectangular cylinder; Separation; Reattachment; Flow visualization; Turbulence; Strouhal number

1. Introduction

It is well known that the aerodynamic characteristics of rectangular cylinders change drastically with width/height ratio, c/d. As the ratio c/d increases, the variation of drag coefficient of the cylinder shows a sharp peak for c/d of about 0.67, and the Strouhal number increases discontinuously with c/d near 2.8. The above-mentioned phenomena were reported by Nakaguchi et al. (1968), and later confirmed by Bearman and Truman (1972) and Igarashi (1985a). Okajima et al. (1983) reported that the Strouhal number changes drastically with c/d for c/d of about 6.0. Igarashi (1985a) experimentally investigated the flow behavior around rectangular cylinders at an angle of attack of 0°. Igarashi (1986a, 1987) also studied the local heat transfer characteristics around rectangular cylinders for c/d in the range 0.33–4.0. The flow and local heat transfer characteristics around a square prism at some angle of attack were experimentally investigated by Igarashi (1984, 1985b, 1986b).

The rectangular cylinder with $c/d \geqq 10$ represents louvered fins and offset fins of heat exchangers. In order to develop a high-performance heat exchanger, recently, experiments (Tanaka et al., 1983) and numerical simulations (Suzuki et al., 1989; Xi et al., 1989) on flow and heat transfer characteristics of various types of fins were carried out to have a clear understanding of this phenomena. According to Tanaka et al. (1983), the optimum inclined angle of louvered, corrugated-fin heat exchangers is 5°. Moreover, there are several papers that have reported the results of studies on inclined-plate solar collectors (Sparrow and Tein, 1977) and on local heat transfer behavior on the flow separated–reattachment surface of a model rectangular cylinder with a sectional width/height ratio of 4–10 (Test and Lessmann, 1980; Motwani et al., 1985). Nevertheless, the results of these studies did not help to have a clear understanding of the interlink between fluid flow and local heat transfer.

The objective of the present experimental studies is to obtain basic knowledge about the local and average heat transfer from the rectangular cylinder with a section c/d of 5.0 and a small inclination angle. Emphasis is given on the studies of heat transfer behavior in the region of separated and reattached flow and on the correlation between heat transfer coefficients in the region of separated flow and the fluctuating pressure coefficients. Comparison is made with those reported in the previous work (Igarashi, 1986a; Igarashi and Hirata, 1974).

2. Experimental apparatus and procedure

The coordinate system and the symbols used in the representations are presented in Fig. 1. Experiments were carried out in a low-speed, 2-D blown-type wind tunnel with a test section having cross-section area of 400 mm × 150 mm and a

* Corresponding author.
E-mail address: tigarash@nda.ac.jp (T. Igarashi).

0142-727X/01/$ - see front matter
PII: S0142-727X(01)00089-3

Nomenclature

C	parameter
c, d	width and height of section of rectangular cylinder
Cp_b	base pressure coefficient
Cp'	fluctuating pressure coefficient, $\Delta p/0.5\rho U^2$
d^*	projected width of rectangular cylinder
d_w	wake width defined by distance between two shear layers
f	vortex shedding frequency
h, h_x	local heat transfer coefficient
h_m	overall heat transfer coefficient
$\bar{h}$	average heat transfer coefficients on each face
Nu, Nu_x	local Nusselt numbers, $hd/\lambda, h_x d/\lambda$
$\overline{Nu}$	average Nusselt numbers, hd/λ
Nu_m	overall Nusselt numbers, $h_m d/\lambda$
$\overline{Nu}_b\overline{Nu}_{bc}$	average Nusselt number on rear face, $\overline{Nu}_b = \bar{h}_b d/\lambda, \overline{Nu}_{bc} = \bar{h}_{bc}/\lambda$
Δp	root mean square value of fluctuating pressure
Re	Reynolds number, Ud/v
Re_c, Re_x	Reynolds number appearing in Fig. 2, $Re_c = Uc/v, Re_x = U_\infty x/v$
S	Strouhal number, fd/U
S^*, S^{**}	modified Strouhal number, $S^* = fd^*/U$, $S^{**} = fd^*/U_s$
U	free stream velocity
U_∞	velocity at the outer boundary layer
U_s	velocity along free stream line at separation point, $U\sqrt{1 - Cp_b}$
$\bar{u}$	time-averaged velocity
Δu	root mean square value of fluctuating velocity
x	distance from forward stagnation point
x_R, x_S	reattachment and separation points

Greek symbols

α	angle of attack
λ	thermal conductivity of fluid
v, ρ	viscosity and density of fluid

Subscripts

b, f	rear and front faces
R, s	reattachment (bottom) and side (top) faces
m	overall

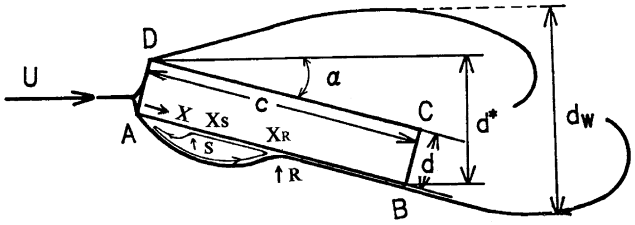

Fig. 1. Coordinate system and symbols.

length of 800 mm. The model rectangular cylinder used in the experiment was of chord length, c, of 50 mm, a thickness, d, of 10 mm shown in Fig. 1 and an axial length normal to the flow of 150 mm. The attack angle of the cylinder, α, varied from 0° to 20°. The tunnel blockage ratio ranges from 0.025 to 0.066, therefore, the effects of tunnel blockage on the characteristics on fluid flow and heat transfer can be neglected (Igarashi and Hirata, 1974). The temperature of free stream is nearly 20°C. The uniform free-stream velocity U was varied from 4 to 20 m/s, which corresponded to Reynolds numbers, Re, defined on the basis of the thickness of the rectangular cylinder d as the reference length, in the range 2560–12 800. In the above-mentioned velocity range, the free-stream turbulence intensity was about 0.4%. At first, the flow pattern around the rectangular cylinder was visualized by using a smoke tunnel and the surface flow pattern was visualized on the basis of the oil-film method. The time-averaged velocity $\bar{u}$ and the turbulence intensity Δu in the outside of shear layers separated from the rectangular cylinder were measured by using an I-type hot-wire anemometer. Several pressure tappings of 0.6 mm diameter were employed along the surface of the rectangular cylinder. The distribution of pressure coefficients, Cp, on the surfaces AB and CD and the base pressure coefficient, Cp_b, at the center of the surfaces BC and CD in Fig. 1 were measured by a manometer, and the fluctuating pressure coefficient, Cp', was measured with a semi-conductor pressure sensor, connected to pressure taps on the center of the surfaces AB, CD and BC, through a stainless tube 1.0 mm in diameter and 50–100 mm long. The phase lag in the measurements of fluctuating pressure can be neglected (Igarashi, 1984). The Strouhal numbers corresponding to the vortex shedding from the rectangular cylinder were determined from frequency analysis of the fluctuating velocity in separated shear layer. The test model used in measurement of the heat transfer was made of acrylic resin, the entire surface of which was coated with stainless foil having a thickness of 0.01 mm. Electrodes were installed at both ends. This was heated by supplying electric power to attain a constant heat flux condition. The wall temperature was measured by copper–constantan thermocouples of $\phi = 0.1$ mm. The thermocouples were embedded on the wall surface with a gap of 2–3 mm.

The experimental uncertainties were calculated using standard uncertainty analysis methods (Kline, 1985). The uncertainty in the temperature ranged from 1% to 2% of the wall-to-freestream temperature difference depending on the operating temperatures, and the uncertainty for the surface heat flux was 2%. The calculated uncertainties for the convective heat transfer coefficient values range from 2.2% to 2.8%.

As a preliminary test of measurements of the pressure and local heat transfer coefficients, the laminar flow heat transfer in the front surface of the rectangular plate normal to air-stream was measured and compared with theoretical value. As shown in Fig. 2, it was confirmed that the measurement accuracy of the heat transfer coefficient of this model was within 5%. The heat transfer in the region of flow separation on the rear surface of the rectangular plate was also measured. It can be observed from Fig. 2 that the results obtained by the present experiment agreed quite well with those reported in the papers (Igarashi and Hirata, 1974; Igarashi, 1985b). The two Reynolds numbers, Re_x and Re_c, and two Nusselt numbers, Nu_x and $\overline{Nu}_{bc}$, are defined in the nomenclature section.

3. Experimental results and discussion

3.1. Flow visualization

Fig. 3 shows the results of smoke tunnel flow visualization around the rectangular cylinder for $Re = 3850$. The pictures (a) and (b) were taken under long, 1 s, and instantaneous expo-

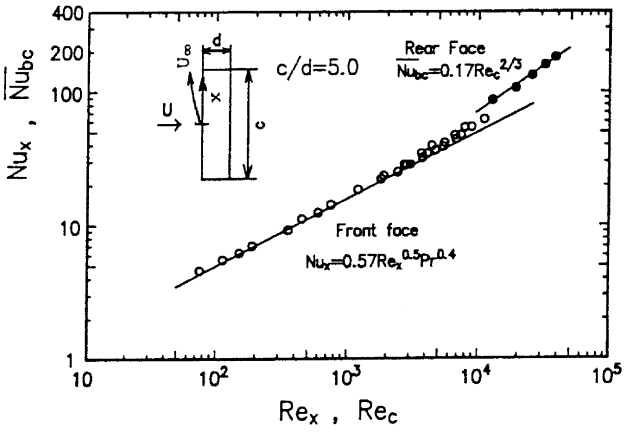

Fig. 2. Accuracy of the measurement of the local heat transfer. ○: $Nu_x = h_x/\lambda, Re_x = U_\infty x/\nu$. ●: $Nu_{bc} = \bar{h}_{bc}/\lambda, Re_c = U_c/\nu$.

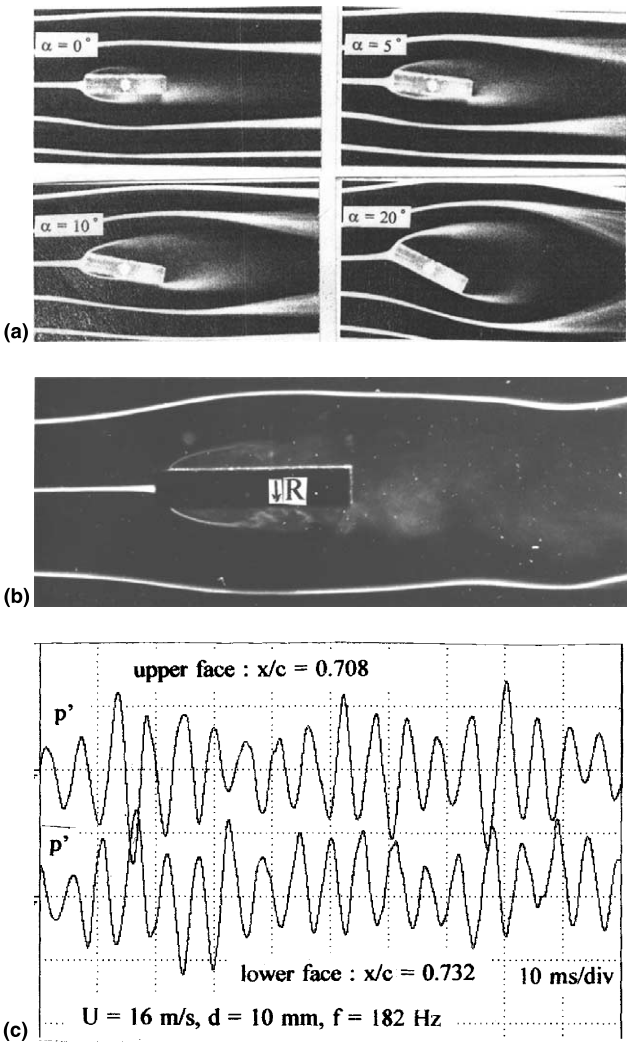

Fig. 3. Visualization of the flow around the cylinder using smoke tunnel and pressure fluctuation on the reattachment region. (a) Long exposure (1 s): $Re = 3850$. (b) Instantaneous exposure: $\alpha = 0°$, $Re = 3850$. (c) Pressure fluctuations on the upper and lower faces: $\alpha = 0°$, $Re = 10000$.

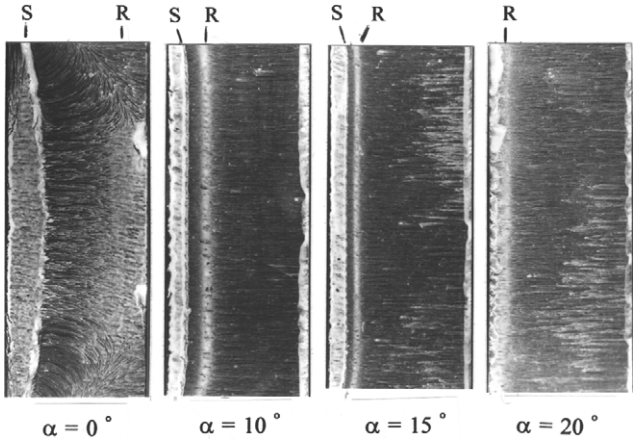

Fig. 4. Surface oil-flow patterns on the reattachment face at $Re = 10000$.

sures, respectively. Fig. 3(c) shows the pressure fluctuations on the center of the upper and lower surfaces AB and CD. The upper and lower waves are out of phase by half a period each other. Fig. 4 shows the surface oil-flow pattern of the lower surface AB of the rectangular cylinder. At $\alpha = 0°$, both the shear layers get separated from the front edges A and D, then reattached on the side wall surface near the trailing edge of the rectangular cylinder (R) and the separation bubbles are formed on the upper and lower surfaces. As shown in Figs. 3(b) and (c), such a flow reattachment process is not steady, but occurs periodically. The separation line (S) appears in the location where separation bubbles are formed. This separation line for $\alpha = 0°$ in Fig. 4 is not straight and is curved near the both end walls. The oil-flow pattern show the end effect caused by the formation of horseshoe vortices. For $\alpha \geqq 5°$, the upper shear layer does not get reattached on the upper surface DC. The wake width, d_w, in Fig. 1 defined by the distance between the two shear layer increases with α. The region of vortex formation, which is defined as the position of rolling up of the shear layer separated from the rectangular cylinder, moves downstream until $\alpha = 15°$ and gets close to the rectangular cylinder for $\alpha = 20°$. The lower side shear layer reattaches steadily and the reattachment line moves forward with the increase in α. Variations of the location of reattachment, x_R, on the lower surface AB of Fig. 1, the separation point, x_S, shown in Fig. 1 in the region where separation bubbles are formed and the wake width, d_w, with α are presented in Fig. 5. The value of x_S/d is nearly one half of x_R/d, similar to that observed with a square prism (Igarashi, 1984). The reattachment and separation lines are clear particularly for $\alpha = 5°$ and 10°. The separation bubble becomes smaller with the increase in α.

3.2. Mean velocity and turbulence distributions

The results on the distributions of mean velocity, $\bar{u}/U$ and turbulence intensity, $\Delta u/U$, around rectangular cylinder are presented in Fig. 6, and the trace of the location corresponding to the maximum turbulence intensity, that is, the center of the shear layer are indicated by the dotted line in the same figure. In the case of $\alpha = 0°$, the traces are parallel to the wall surface downstream of the reattachment point. The maximum values of turbulence intensity above 20% and about 10–15% were exhibited in the vicinity of the wall. For $\alpha \geqq 5°$, the turbulence intensity in the vicinity of the lower wall was above 20% in the region downstream of the location of reattachment. As the attack angle α is increased, the leading edge separation bubble

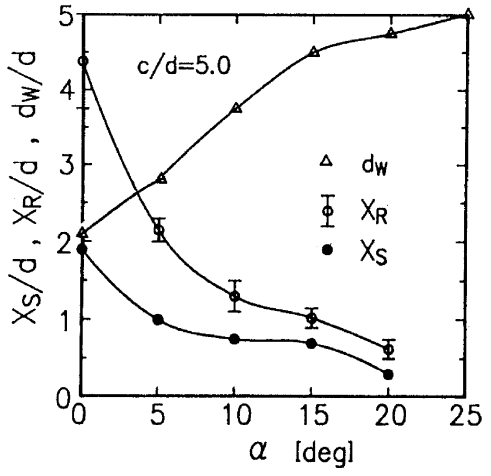

Fig. 5. Variations of wake width and reattachment point with α.

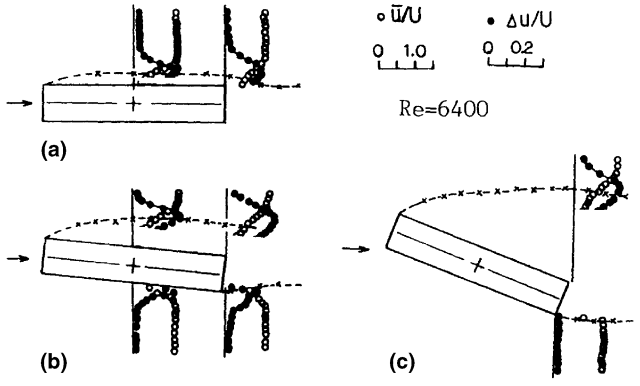

Fig. 6. Distributions of mean velocity and the rms velocity fluctuations.

becomes smaller and consequently the turbulence intensity decreases gradually. For $\alpha = 20°$, the turbulence intensity in the region of reattachment flow becomes less than 1%, and the flow becomes laminar.

3.3. Base pressure coefficient and fluctuating pressure coefficient

The base pressure and fluctuating pressure at the center of the rear surface BC are closely related to the fluid flow and heat transfer phenomena in the region of separation (Igarashi and Hirata, 1974; Igarashi, 1986a, 1987). In the present experiments, the variations of the base pressure coefficient and fluctuating pressure coefficient at the center of the surface BC, Cp_b and Cp', with the angle of attack, α, are displayed in Fig. 7. The negative value of Cp_b increases proportionally to α in the range 0–10° and $\alpha \geqq 15°$. Such a decrease in the base pressure Cp_b corresponds to an increase in the projected width or the wake width of the rectangular cylinder, d^* or d_w. The fluctuating pressure coefficient, Cp', increases abruptly for certain α and shows a peak at about $\alpha = 5°$, then decreases suddenly. For α above 10°, the value of Cp' is lower than that for $\alpha = 0°$. The variation of Cp' is related to the length between the region of vortex formation to the rear surface BC (Igarashi, 1986a, 1987). Namely, the value of Cp' exhibits a peak for $\alpha = 5°$, when the region of vortex formation approach close to the rear surface BC of Fig. 1 of the rectangular cylinder. Therefore, it is

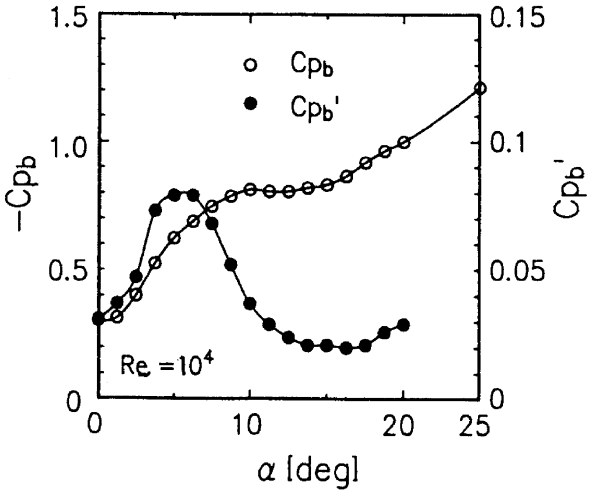

Fig. 7. Base pressure coefficient and fluctuating pressure coefficient.

expected that the heat transfer on the rear surface BC of the rectangular cylinder will have the maximum value for $\alpha = 5°$.

3.4. Strouhal number

Fig. 8 presents the variation of Strouhal number, S, with α. The value of S, defined as fd/v, is nearly constant for $\alpha \leqq 5°$ and decreases with increases in α for $\alpha > 5°$. We attempt to obtain a new interpretation about the Strouhal number. Thereupon two Strouhal numbers, $S^* = fd^*/U$, and the modified Strouhal number, $S^{**} = fd^*/U_s$, were defined, where the reference length is the projected width d^* and U_s is the maximum velocity in the shear layer at the point where the flow separates from the reattachment surface AB of Fig. 1. Namely, U_s is defined by Bernoulli's theorem, $U\sqrt{1 - Cp_b}$. The results obtained from this rearrangement are also presented in Fig. 8. The value of S^* increases with α for α less than 10° and has a constant value of 0.19 for α in the range 10–20°. This tendency is generally evident in the case of square prism (Igarashi, 1984). It can be considered that the decrease of the vortex shedding frequency f for $\alpha = 10$–20° was mainly caused by the increase in projected width d^* of Fig. 1, of the rectan-

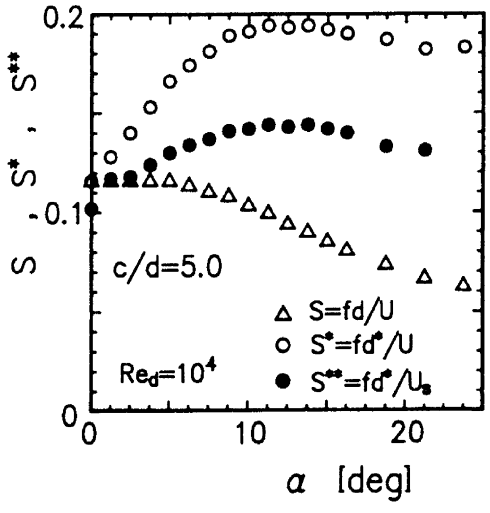

Fig. 8. Strouhal number.

gular cylinder. The modified Strouhal number S^{**} is about 0.14 for α in the range 10–20°. For α at about 10°, on the bottom surface AB of Fig. 1, the shear layer separates at the leading edge A on Fig. 1, reattaches in the downstream region and undergoes transition to laminar flow near the trailing edge.

3.5. Local heat transfer coefficients

The variations of the distribution of local heat transfer coefficient around the rectangular cylinder with α are shown in Figs. 9(a)–(d). The value of heat transfer coefficient h is readily convertible into the Nusselt number $Nu = hd/\lambda$, that is, $Nu = 0.381 \times h$ [W/m^2 K]. For $\alpha = 0°$, the heat transfer coefficients on the front surface exceed those of the rear surface. The comparison is contrary to that in the case of a width/height ratio, c/d, of 4 (Igarashi, 1986a). This is because the reattachment region moves forward from the trailing edge as the ratio c/d increases from 4 to 5 and fluctuating pressure and velocity drop strongly in the wake region. As a result, the heat transfer coefficient on the rear surface decreases. The heat transfer coefficients on the upper and lower surfaces have a maximum value at the reattachment point (R) and a minimum value at a location just before the separation point (S) in the region where separation bubbles are formed. The gentle peak in the profile for $\alpha = 0°$ is in contrast to the sharp peaks observed in the cases of α values of 5° and 10°. This is caused by the above-mentioned difference in the flow behavior between intermittent reattachment and steady reattachment. As α is increased, the stagnation point on the front surface, DA of Fig. 1, which corresponds to the location of peak heat transfer coefficients, approaches the leading edge, A of Fig. 1. On the contrary, the location of peak heat transfer coefficient in the region of flow separation, surface DC of Fig. 1, corresponds to the trailing edge C of Fig. 1, nearest to the region of vortex formation. The sharp peak in the distribution of heat transfer coefficient is symmetric with respect to the corner C on the both surfaces BC and CD. The peak value has exceeded the heat transfer coefficient at the reattachment point x_R of Fig. 1, where denoted by "R" in Fig. 9. The variations of distribution of heat transfer coefficient on the reattached and separated surfaces, AB and CD, with α are presented in Figs. 10(a) and (b), respectively. In the cases of $\alpha = 5$–20°, the heat transfer coefficient on the separated surface CD has a maximum at the tail corner C and decreases toward to the leading edge corner D. The heat transfer coefficients decrease with increase in α. This is thought to be due to the spread of the wake and the movement of the location of vortex formation downstream with increase in α, as shown in Fig. 3. In the case of $\alpha = 5°$, the heat transfer coefficient on the reattached surface AB increases in the forward from the reattachment region compared with that for $\alpha = 0°$. For $\alpha = 10°$, the heat transfer coefficient on the surface AB has a maximum at the reattachment point, then

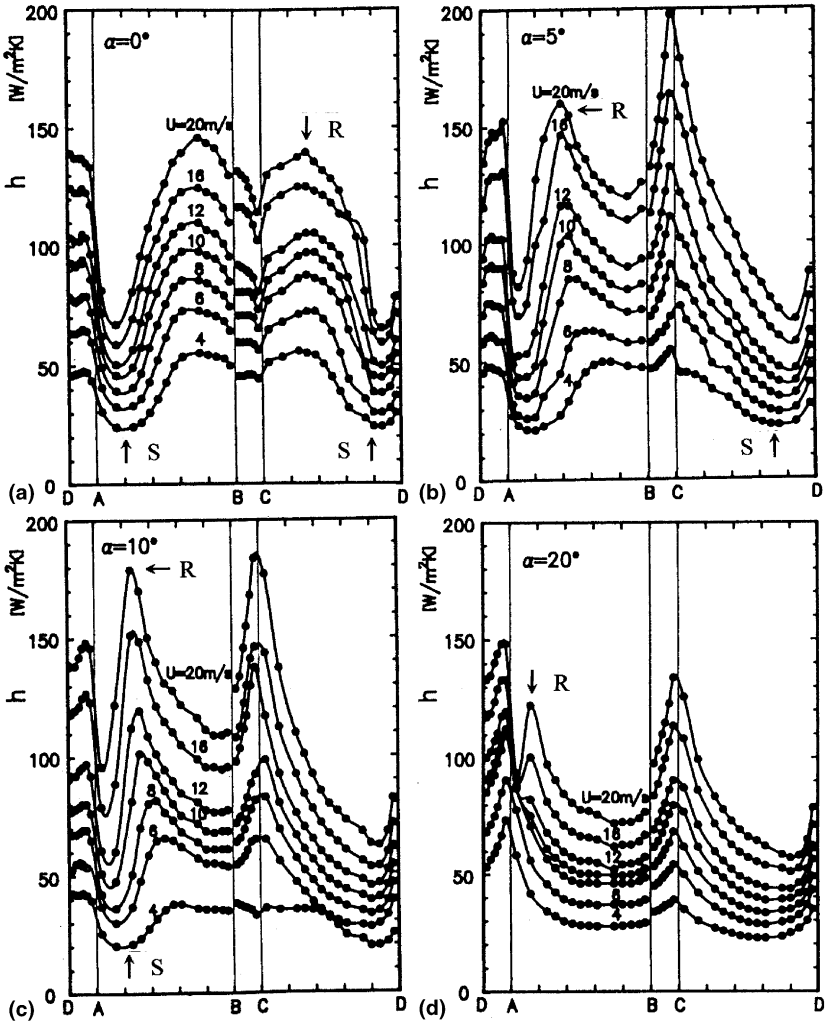

Fig. 9. Local heat transfer.

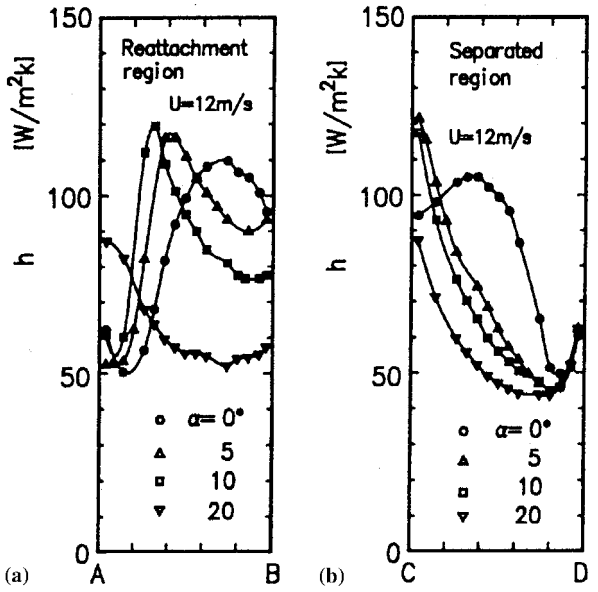

Fig. 10. Variation of the local heat transfer profile with α.

decreases toward the tail corner B. In the case of $\alpha = 20°$, the profile of distribution of the heat transfer coefficient is symmetric with respect to the corner C, in the same manner as that of a square prism (Igarashi, 1986b). The local heat transfer coefficients decreases while surface compared with those for $\alpha < 20°$. This drop in heat transfer coefficients on the reattachment surface is related to the behavior of shear layer separated from the front edge A, which in turn results in a decrease in turbulence intensity in the reattachment flow shown in Fig. 6.

3.6. Average heat transfer coefficient

In this section, the dependencies of the average heat transfer coefficients on each individual surface on Reynolds number are investigated. Figs. 11(a) and (b) present the variations of average Nusselt number on the surface AB, where the flow reattaches, and those on each of the other surfaces for $\alpha = 20°$. On surface AB, the Nusselt number, $\overline{Nu}_R$ except for $\alpha = 20°$ does not satisfy the empirical relation for the laminar flow $\overline{Nu}_f = C_f Re^{0.50}$. The flow on the surface AB changes from separated–reattachment flow to laminar wedge flow with the increase in α. The average Nusselt number can be written as follows:

$$\overline{Nu}_R = C_R Re^{2/3} \quad (\alpha < 15°), \tag{1a}$$

$$\overline{Nu}_R = C_R Re^{1/2} \quad (\alpha = 20°). \tag{1b}$$

The top and rear surfaces are always exposed to a separated flow, therefore those Nusselt numbers satisfy the same relation as $\overline{Nu} \propto Re^{2/3}$, reported in the papers (Igarashi and Hirata, 1974; Igarashi, 1985b, 1986a, 1987).

$$\overline{Nu}_b = C_b Re^{2/3} \quad (\alpha = 0\text{–}20°), \tag{2}$$

$$\overline{Nu}_s = C_s Re^{2/3} \quad (\alpha = 5\text{–}20°). \tag{3}$$

The variations of the above parameters C_R, C_b and C_s with α are plotted in Fig. 12. In the same figure, the estimated value of C_b, which will be discussed later, is also represented by the symbol □. For $\alpha = 0°$, the heat transfer enhancement occurs at the top and bottom surfaces due to the separated–reattachment flow. On the contrary, that for $\alpha = 5°$ is caused by the

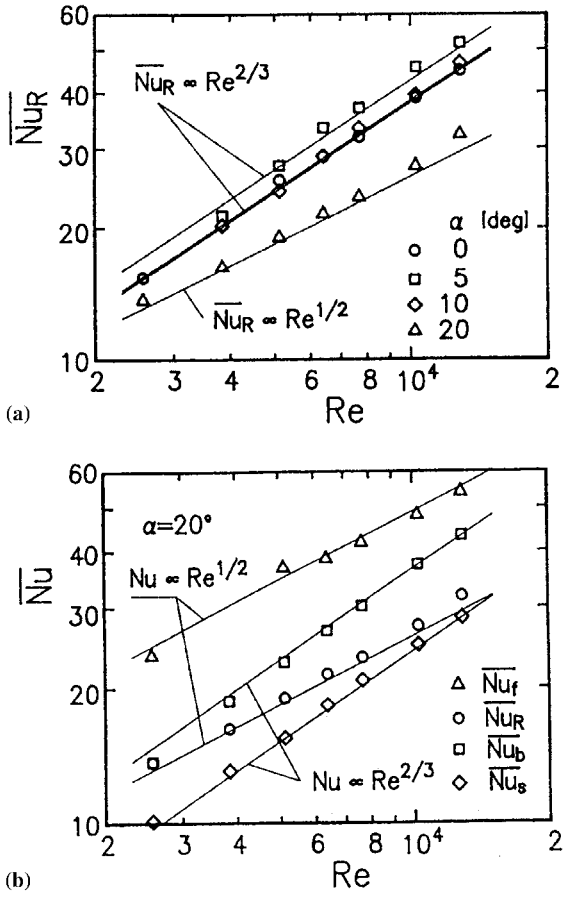

Fig. 11. Average heat transfer on each surface △ $\overline{Nu}_f$ – front face DA; ○ $\overline{Nu}_R$ – reattachment (bottom) face AB; □ $\overline{Nu}_b$ – rear face BC; ◇ $\overline{Nu}_s$ – side (top) face CD.

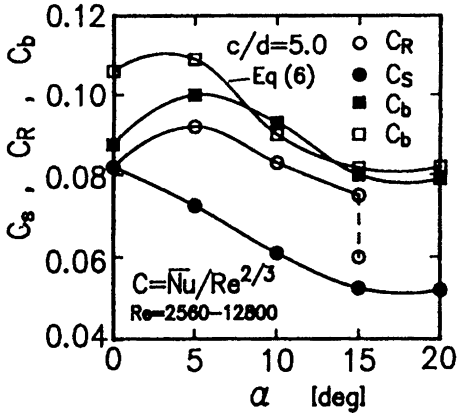

Fig. 12. Variation of the constants C_s, C_R and C_b for the average heat transfer on each face. ○ C_R – reattachment face AB; ● C_s – side (top) face CD; ■ C_b – rear face BC; □ C_b – estimated values obtained from Eq. (6).

turbulent reattached flow on the lower surface. For $\alpha > 5°$, the average Nusselt number on each individual surface decreases with increases in α. The overall Nusselt number, Nu_m, is presented in Fig. 13. The following correlation is proposed:

$$Nu_m = C_m Re^{2/3} \quad (\alpha = 0\text{–}10°,\ Re > 4 \times 10^3). \tag{4}$$

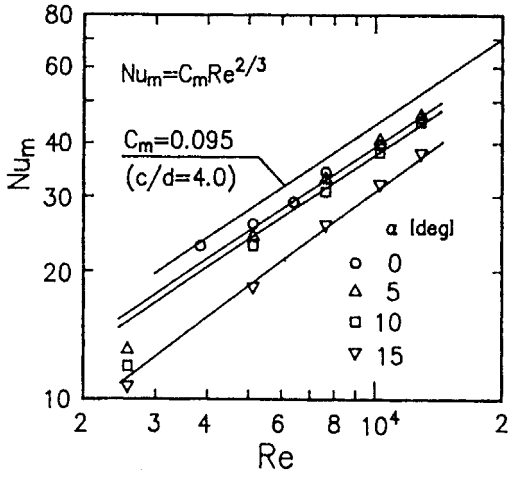

Fig. 13. Overall heat transfer.

In the range $\alpha = 0$–$5°$, the value of $C_m = 0.085$, which is slightly smaller than 0.095 used for the case of $c/d = 4$ (Igarashi, 1986a). The overall heat transfer has a maximum at $\alpha = 5°$. The results of the present study agree well with those reported by Tanaka et al. (1983). They concluded that the optimum angle of attack for the case of inclined louvered-fin heat exchanger is 5°. Furthermore, this optimum angle leads to achieving the maximum heat transfer due to the separated–reattachment flow and is independent of the width/height ratio, c/d, of the rectangular cylinder.

3.7. Correlation between heat transfer and fluctuating pressure in separated region

Igarashi and Hirata (1974) reported that the heat transfer coefficient in separated flows can be closely correlated to the flow parameters, d_w/d and U_s/U. The average Nusselt number $\overline{Nu}_b$ and constant C_b on the rear surface BC is represented by the following general equations:

$$\overline{Nu}_b = 0.10[2/(d_w/d)]^{1/3}[(U_s/U)Re]^{2/3}, \quad (5)$$

$$C_b = 0.126[(1 - Cp_b)/(d_w/d)]^{1/3}. \quad (6)$$

Substitute the experimental results presented in Figs. 5 and 6 into Eq. (6), the values of C_b for different angle of attack are calculated and shown using symbol □ in Fig. 12. The calculated value is slightly higher than the present measured value in the case of $\alpha = 0°$ and 5°, but agrees satisfactorily with the measured value for $\alpha \geqq 10°$. The heat transfer coefficient in the region of flow separation can also be closely related to the fluctuating pressure coefficient, Cp' (Igarashi, 1986a,b, 1987). In the cases of $\alpha = 0°$ and 5°, the results of calculation using the empirical relation between the Nusselt number and new dimensionless number, $\sqrt{Cp'}Re$, are plotted in Fig. 14. The solid line in this figure represents the results reported in the paper (Igarashi, 1986a) for the case of c/d in the range 2.0–4.0 and $\alpha = 0°$. The empirical relation can be written in the following form:

$$\overline{Nu}_b = 1.4(\sqrt{Cp'}Re)^{0.46}. \quad (7)$$

The present experimental data agree approximately with those calculated by using Eq. (7).

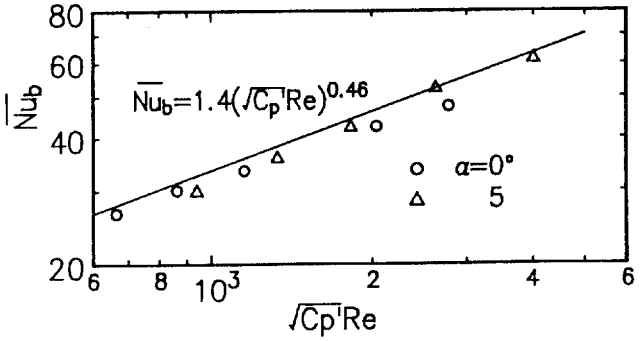

Fig. 14. Correlation between heat transfer on the rear face and fluctuating pressure coefficient.

4. Conclusions

Experimental studies on the fluid flow and heat transfer phenomena around rectangular cylinder having width/height ratio c/d of 5 using air as working fluid were carried out for Reynolds number, Re in the range 2600–12 800. The angle of attack was varied from 0° to 20°. The results led to the following conclusions.

1. At $\alpha = 0°$, the behavior of the separated–reattachment flow on the top and bottom surfaces is periodic. For α above 5°, the reattachment flow on the bottom surface becomes stable and the flow on the top surface becomes fully separated flow.
2. On the surface, where flow reattachment occurs, the turbulence intensity in the region downstream the location of reattachment exceeds 20%. However, for $\alpha \geqq 15°$, the reattached flow become laminar, because the separation bubbles formed at the leading edge becomes smaller.
3. The heat transfer on the front face for $\alpha < 20°$ is not laminar in nature, because of the fluctuation of the front stagnation point.
4. The heat transfer on the bottom surface for $\alpha > 5°$ decreases with the increase in α. The Nusselt number Nu is proportional to $Re^{2/3}$ for α in the range of 0° to 15°, due to the separated–reattachment flow. Whereas Nu is proportional to $Re^{1/2}$ for $\alpha = 20°$, due to its similarity with wedge flow.
5. The heat transfer coefficients on the rear and top surfaces, where flow separation occur, decrease with the increase in α, and the corresponding Nusselt numbers Nu are proportional to $Re^{2/3}$. In the case of $\alpha \geqq 10°$, the heat transfer coefficients on the rear surface agree well with the result in the region of flow separation for bluff body reported in a previous paper.
6. The heat transfer coefficient on the rear surface for $\alpha = 0°$ and 5° is almost equal to that obtained by the following empirical equation, which is developed for rectangular cylinder having c/d in the range 2–4 and $\alpha = 0°$ on the basis of the rms fluctuating pressure coefficient

   $$\overline{Nu}_b = 1.4(\sqrt{Cp'}Re)^{0.46}.$$

7. Setting of $\alpha = 5°$ leads to the maximum overall heat transfer coefficient.

References

Bearman, P.W., Truman, D.M., 1972. An investigation of the flow around rectangular cylinders. Aero. Q. 23, 229–237.

Igarashi, T., 1985a. Characteristics of the flow around rectangular cylinders (the case of the angle of attack 0 deg). Bull. JSME 28 (242), 1690–1696.

Igarashi, T., 1987. Fluid flow and heat transfer around rectangular cylinders (the case of a width/height ratio of a section of 0.33–1.5). Int. J. Heat Mass Transfer 30 (5), 893–901.

Igarashi, T., 1986a. Fluid flow and heat transfer around rectangular cylinders (the case of a width/height ratio of a section of 2.0–4.0). Trans. Jpn. Soc. Mech. Engrs. B 52 (480), 3011–3016.

Igarashi, T., 1984. Characteristics of the flow around a square prism. Bull. JSME 27 (231), 1858–1865.

Igarashi, T., 1985b. Heat transfer from a square prism to an air stream. Int. J. Heat Mass Transfer 28 (1), 175–181.

Igarashi, T., 1986b. Local heat transfer from a square prism to an airstream. Int. J. Heat Mass Transfer 29 (5), 777–784.

Igarashi, T., Hirata, M., 1974. Heat transfer in separated flows. Proc. Int. Heat Transfer Conf. 2, 300–304.

Kline, S.J., 1985. The purposes of uncertainty analysis. Trans. ASME J. Fluid Eng. 107, 153–160.

Motwani, D.G., Gaitonde, U.N., Sukhatme, S.P., 1985. Heat transfer from rectangular plates inclined at different angles of attack and yaw to an air stream. Trans. ASME J. Heat Transfer 107, 307–312.

Nakaguchi, H., Hashimoto, K., Muto, S., 1968. An experimental study on aerodynamic drag of rectangular cylinders. J. Jpn. Soc. Aeronaut. Space Sci. 16 (168), 1–5.

Okajima, A., Sugitani, K., Mizota, T., 1983. Strouhal number and base pressure coefficient of rectangular cylinders (the case of a section of a width/height ratio of 1–9). Trans. Jpn. Soc. Mech. Engrs. B 49 (447), 2551–2558.

Sparrow, E.M., Tien, K.K., 1977. Forced convection heat transfer at an inclined and yawed square plate – application to solar collectors. Trans. ASME J. Heat Transfer 99, 507–512.

Suzuki, K., Hayashi, T., Schuerger, M.J., Nishihara, A., Hayashi, M., 1989. Heat transfer characteristics of two-dimensional model of parallel louver fin. Trans. Jpn. Soc. Mech. Engrs. B 55 (516), 2457–2464.

Tanaka, T., Itoh, M., Kudoh, M., Tomita, A., 1983. Development of inclined louver-fin heat exchangers. Trans. Jpn. Soc. Mech. Engrs. B 49 (442), 1204–1213.

Test, F.L., Lessmann, R.C., 1980. An experimental study of heat transfer during forced convection over a rectangular body. Trans. ASME J. Heat Transfer 102, 146–151.

Xi, G., Suzuki, K., Hagiwara, Y., Murata, T., 1989. A basic study on heat transfer characteristics of offset fin arrays (effect of fin thickness in the middle range of Reynolds number). Trans. Jpn. Soc. Mech. Engrs. B 55 (519), 3507–3514.